Origin of the difference in spin-dependent transport properties between half-metallic $Co_2FeGa_{0.5}Ge_{0.5}$ and $Co_2Mn_{0.5}Fe_{0.5}Si$ with the Ag spacer

Kodchakorn Simalaotao[1,2], Yoshio Miura[2,3*], Yuya Sakuraba[1,2*]

[1]Graduate School of Pure and Applied Sciences, University of Tsukuba, Tennodai, Tsukuba 305-8571, Japan

[2] Research Center for Magnetic and Spintronic Materials, National Institute for Materials Science, 1-2-1 Sengen, Tsukuba 305-0047, Japan

[3]Faculty of Electrical Engineering and Electronics, Kyoto Institute of Technology, Hashikami-cho, Matsugasaki, Sakyo-ku, Kyoto 606-8585, Japan

[*]Corresponding Author: miura@kit.ac.jp and SAKURABA.yuya@nims.go.jp

Current-perpendicular-to-plane giant magneto-resistive (CPP-GMR) devices are promising for next-generation magnetic read heads in hard disk drives due to their low resistance area product compared to tunnel magneto-resistive devices. While $Co_2FeGa_{0.5}Ge_{0.5}$ (CFGG) and $Co_2Mn_{0.5}Fe_{0.5}Si$ (CMFS) are representative half-metallic Co-based Heusler alloys with experimentally observed high magnetoresistance (MR) in CPP-GMR with Ag spacer, there is no understanding of the origin of the different band matching with the Ag spacer for the evaluation of ferromagnetic electrodes. In this study, first-principles calculations of the ballistic conductance in (001)-CFGG/Ag/CFGG and CMFS/Ag/CMFS were performed to clarify an origin of the difference in the spin-dependent conductance. We found that the majority-spin conductance of the CFGG/Ag(001) at its maximum was about 45% higher than that of the CMFS/Ag(001) over all interfacial terminations, indicating the advantageous potential of CFGG for achieving a larger MR ratio in CPP-GMR. The Fermi surface analysis revealed that a hybridization between the *d*-states of the CFGG electrode and the *p*-states of the Ag spacer around the Brillouin Zone edge plays an important role in the Fermi surface matching at the interface. In addition, the calculated exchange stiffness constant revealed that CFGG/Ag(001) interfaces exhibit higher stability to thermal fluctuations of the spin-moment than CMFS/Ag(001) interfaces, indicating suppression of the decrease of the MR ratios at finite temperatures. All these findings provide important insights for the selection of materials for high-performance spintronic devices.

I. INTRODUCTION

A current perpendicular to plane giant magneto-resistive (CPP-GMR) devices have gained much attention for the next generation read head in hard disk drives (HDD) over 2 Tbit/in^2 due to their much smaller resistance area product (RA). A smaller RA of less than 0.2 Ω μm^2 will be required for making a small read head suitable for high-speed reading in HDD compared to tunneling magnetoresistance (TMR) counterparts [1,2]. The CPP-GMR devices consist of two or more ferromagnetic layers separated by a non-magnetic conductive spacer layer, which exhibits the change in electrical resistance to the perpendicular to the film plane direction due to a relative angle of magnetizations in the neighboring ferromagnetic layers. The resistance change area product ($\Delta R\mathrm{A} = R_{\mathrm{AP}}\mathrm{A} - R_{\mathrm{P}}\mathrm{A}$) between antiparallel and parallel magnetization can be described using the two-current series resistor (2CSR) model of up- and down-spin electron channels [3,4]. This model considers two intrinsic factors associated with spin-dependent electron scattering: the bulk spin-asymmetry coefficient (β) and the interfacial spin-asymmetry coefficient (γ). The β is defined as $\beta = \frac{\sigma^{\uparrow}_{\mathrm{bulk}} - \sigma^{\downarrow}_{\mathrm{bulk}}}{\sigma^{\uparrow}_{\mathrm{bulk}} + \sigma^{\downarrow}_{\mathrm{bulk}}}$ within the ferromagnetic layers, where $\sigma^{\uparrow}_{\mathrm{bulk}}$ and $\sigma^{\downarrow}_{\mathrm{bulk}}$ represent the conductivity for the majority and minority spins of bulk, respectively. Similarly, γ is defined as $\gamma = \frac{R^{\downarrow}_{\mathrm{int.}}\mathrm{A} - R^{\uparrow}_{\mathrm{int.}}\mathrm{A}}{R^{\downarrow}_{\mathrm{int.}}\mathrm{A} + R^{\uparrow}_{\mathrm{int.}}\mathrm{A}}$ for the interface, with the $R^{\downarrow}_{\mathrm{int.}}\mathrm{A}$ and the $R^{\uparrow}_{\mathrm{int.}}\mathrm{A}$ denoting the resistance area product for minority and majority spins at interface between ferromagnetic (FM) layers and nonmagnetic (NM) spacer, respectively. Enhancing β and γ parameters by selecting proper materials for FM electrode and NM spacer increases the magnetoresistance (MR) ratio in CPP-GMR devices. Practically, β can be maximized by utilizing half-metallic materials as a FM layer due to its 100% spin polarized electronic structure at the Fermi level. On the other hand, γ can be enhanced by choosing the suitable combination of FM electrode and NM spacer which has a spin-asymmetric electronic band matching that increases $R^{\downarrow}_{\mathrm{int.}}\mathrm{A}$ and reducing $R^{\uparrow}_{\mathrm{int.}}\mathrm{A}$. Since there are no states around the Fermi level of half-metallic minority-spin states in the bulk resulting in a finite value for $R^{\downarrow}_{\mathrm{int.}}$ in the FM/NM junctions, achieving a high MR ratio depends on choosing a ferromagnetic material with a suitable non-magnetic spacer material that enlarges $R^{\uparrow}_{\mathrm{int.}}\mathrm{A}$ to maximize γ parameter.

In previous studies, the use of half-metallic Heusler alloy as an electrode, renowned for its high magnetoresistance (MR) ratio [5–10], has garnered significant attention in the field of

spintronics. Co-based full-Heusler alloys are emerging as highly promising materials for various spintronic devices due to their exceptional properties. Remarkably high magnetoresistance (MR) ratios, exceeding 30% at room temperature (RT), have been achieved in devices utilizing Co-based full-Heusler alloy electrodes such as Co_2MnSi [11,12], $Co_2Mn_{0.5}Fe_{0.5}Si$ [5,13–15], and $Co_2FeGa_{0.5}Ge_{0.5}$ [5,16–18] in conjunction with Ag or Ag-based non-magnetic alloy spacers in the CPP-GMR configurations. Such performance levels are unprecedented in devices using conventional ferromagnets, underscoring the potential importance of Co-based full-Heusler alloys in advancing spintronics technology. However, further improvement of the MR properties is still required for next generation read head application.

Taking advantage of first-principles calculations, we can reveal the physical properties of the designed CPP-GMR materials and evaluate their innovative functionalities [19,20]. For example, a study aimed at understanding the origin of the difference in γ between Co_2MnSi/Ag/Co_2MnSi and Co_2MnSi/Cr/Co_2MnSi was clarified through first-principles ballistic conductance calculations [11]. The findings indicate that the majority-spin resistance area product of Co_2MnSi/Ag/Co_2MnSi (~3.21 mΩ μm^2) is significantly smaller than that of Co_2MnSi/Cr/Co_2MnSi (~16.1 mΩ μm^2), which is in good agreement with experimental observations. This agreement serves as evidence of a reduced interface resistance and an enhanced γ between Co_2MnSi and Ag due to a good Fermi-surface matching, as predicted theoretically. Consequently, the reported MR ratio of Co_2MnSi/Ag/Co_2MnSi stands at 36.4% [11], significantly higher than the 2.4% MR ratio [21] observed for Co_2MnSi/Cr/Co_2MnSi at room temperature. In addition, the experiment confirmed the larger γ at the Co_2MnSi/Ag interfaces compared to that at the Co_2MnSi/Cr interface, using the same stacking structure [12].

There are critical underlying factors regarding the physical origin of the differences observed in Co-based full-Heusler alloy electrodes. These include a lack of understanding of the underlying potential of electrode evaluation and the primary reasons for selecting suitable electrode materials along with an appropriate spacer. Interestingly, researches on CPP-GMR measurements have reported comparable high MR ratio in $Co_2FeGa_{0.5}Ge_{0.5}$(CFGG)/Ag/$Co_2FeGa_{0.5}Ge_{0.5}$(001) [16] system, reaching 57% and in $Co_2Mn_{0.5}Fe_{0.5}Si$(CMFS)/Ag/$Co_2Mn_{0.5}Fe_{0.5}Si$(001) [13] system, achieving 58% at room temperature. Nevertheless, the reported theoretical $R^{\uparrow}_{\mathrm{int.}}$A values [22], which represent the spin-

dependent transport properties, differ significantly between CFGG/Ag/CFGG (~4.42 mΩ μm^2) and CMFS/Ag/CMFS (~5.75 mΩ μm^2) systems, and remain unclear from a theoretical standpoint. Although the CFGG and CFMS are two of the representative half-metallic Heusler alloys that showed the experimental highest MR ratios in the CPP-GMR, there has been no experimental comparative study on CFGG and CMFS so far to clarify which electrode is suitable for an Ag spacer because of the unavoidable difficulty to experiment with the perfectly same conditions. This discrepancy warrants further theoretical investigation to better understand the underlying factors influencing the transport property using these electrodes and determine which CFGG or CFMS is suitable for obtaining larger MR performance.

The purpose of this study is to investigate and clarify the physical origins of the spin-dependent transport properties exhibited by the different electrodes of CFGG and CMFS, with implications for the design of interface structures in CPP-GMR devices. Our study focuses on a fully epitaxial multilayer configuration, where the crystal momentum parallel to the layer ($k_{\parallel}$) remains conserved due to the two-dimensional periodicity of the system. Thus, we employ ballistic transport calculations based on the Landauer formula to evaluate differences in majority-spin interface resistance, while taking into account their interfacial structural stability. In addition, we analyze the transmittance projected onto Ag atomic orbitals at the interface, revealing their specific orbital contribution. To further understand the stability of spin moments against thermal agitation, we study noncollinear magnetic structures in the local spin moments across different interfacial terminations. These results will provide important insights for the selection of materials for high-performance spintronic devices. Furthermore, we intend to focus future research efforts on using first-principles calculations to design CPP-GMR materials with innovative functionalities.

II. COMPUTATIONAL METHOD

According to the two-current series resistor (2CSR) model [4], the interface resistance is strongly spin-dependent and typically dominates the resistance and magnetoresistance for layer thicknesses that are not excessively large [23,24]. Thus, understanding CPP-GMR largely depends on understanding the origin of the interface resistance [25]. Here, it should be noted that in real devices, current flow involves both ballistic and diffusive transport due to scattering at interfaces and material imperfections, which increases resistance and reduces efficiency. However, in the theoretical analysis of CPP-GMR devices, we can minimize the effects of diffusive scattering, because the thickness of the NM spacer layer is much shorter than the mean free path of electrons, approaching ballistic transport, especially in nanoscale systems. Therefore, the Landauer-Büttiker theory is useful for analyzing ballistic transport in atomic-sized contacts, especially in CPP-GMR devices, where interfacial resistance at FM/NM junctions significantly affects the transport properties. Therefore, we perform first-principles ballistic transport calculations based on the Landauer formula [26] to investigate the difference in the interface resistance between CFGG and CMFS electrodes. Our calculations are based on density functional theory (DFT) within the generalized- gradient approximation for the exchange-correlation energy [27]. To perform the interfacial structure optimization, the plane-wave basis sets along with the ultrasoft pseudopotential method are adopted by using the QUANTUM-ESPRESSO code [28]. A set of 10 × 10 × 1 grid of k-points is used for the Brillouin zone integrations. The cutoff energy for the wave function and charge density is set to 40 (Ryd) and 400 (Ryd), respectively. A supercell of $Co_2FeGa_{0.5}Ge_{0.5}$/Ag/$Co_2FeGa_{0.5}Ge_{0.5}$(001) and $Co_2Mn_{0.5}Fe_{0.5}Si$/Ag/$Co_2Mn_{0.5}Fe_{0.5}Si$(001) junctions, namely CFGG/Ag/CFGG(001) and CMFS/Ag/CMFS(001) junctions were constructed in a tetragonal supercell with the in-plane lattice parameters of the supercell are fixed at 4.06 Å and 3.98 Å, respectively. The lattice mismatches between the Ag spacer and each electrode are 1.69% for CFGG and 3.78% for CMFS, respectively. The CFGG/Ag(001) interface has three types of termination, namely FeGa termination, Co termination, and FeGe termination, and of the identical CMFS/Ag(001) interface, namely MnSi termination, Co termination, and FeSi termination. The multilayer supercell consists of 7 atomic layers of the Ag spacer, 21 atomic layers of CFGG/CMFS for the FeGa/MnSi termination, and 17 atomic layers of CFGG/CMFS for the Co and FeGe/FeSi termination. エラー! 参照元が見つかりません。(a-c) shows the supercell of the CFGG/Ag/CFGG(001) junction with FeGa termination, Co termination, and FeGe termination,

respectively, visualized by XCRYDEN [29]. The ballistic conductance was calculated using the Landauer formula with semi-infinite boundary conditions by the method of Choi and Ihm method [30,31]. It should be noted that the spin-orbit scattering can be expected at the CFGG/Ag(001) and CMFS/Ag(001) interfaces, such as the Rashba effect, which can significantly influence magnetization reversal through spin-orbit torque in three-terminal devices with current flow parallel to the FM/NM interface. However, in a CPP-GMR device, which is a two-terminal system with current flowing perpendicular to the FM/NM interface, the Rashba effect is expected to have minimal impact on the CPP-GMR effect. To estimate an exchange stiffness constant at each interfacial termination of CFGG/Ag(001) and CMFS/Ag(001) junctions, we calculated the increase in total energies of the system, denoted as E(θ), with a dependence on the angle of local spin moments, θ, using Vienna Ab initio Simulation Package (VASP) codes [32,33]. Based on the magnetic force theorem method [34,35], the obtained results were fitted using the function $E(\theta) = B(1 - \cos\theta)$, where B represents the inter-atomic-layer exchange stiffness constant.

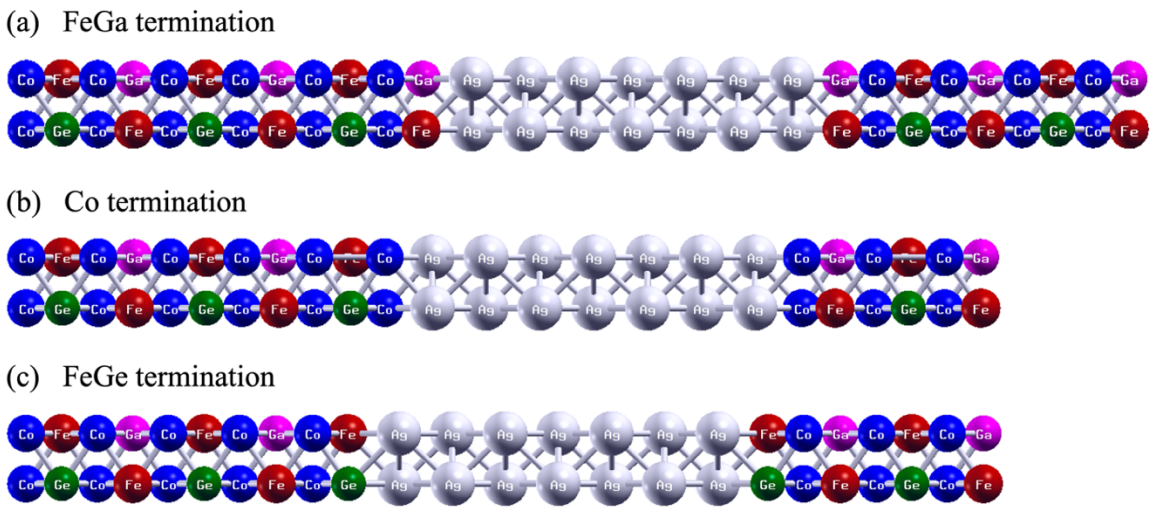

FIG. 1. Supercell of the $Co_2FeGa_{0.5}Ge_{0.5}$/Ag/$Co_2FeGa_{0.5}Ge_{0.5}$(001) junction with (a) FeGa termination, (b) Co termination, and (d) FeGe termination visualized by XCRYDEN [29] and of identical $Co_2Mn_{0.5}Fe_{0.5}Si$/Ag/$Co_2Mn_{0.5}Fe_{0.5}Si$(001) junction with Fe atom replaced by Si atom, Ga atom replaced by Mn atom, and Ge atom replaced by Fe atom.

III. RESULTS AND DISCUSSION

A. Interfacial structure stabilities

We have optimized the interface structure for each termination of CFGG/Ag/CFGG(001) and CMFS/Ag/CMFS(001) junctions by relaxing the atomic positions along the longitudinal direction of the supercell. The optimal interfacial distances are 1.91 Å (Co-termination), 2.01 Å (FeGa-termination) and 2.03 Å (FeGe-termination) for CFGG/Ag/CFGG(001) and 1.95 Å (Co-termination), 1.99 Å (FeSi-termination) and 2.24 Å (MnSi-termination) for CMFS/Ag/CMFS(001), respectively. The formation energy of the two electrodes with each termination was then calculated to evaluate their relative stability. The formation energy for CFGG/Ag/CFGG(001) and CMFS/Ag/CMFS(001) junctions with each termination was determined using the following equation.

$$E_{\mathrm{f}}^{\mathrm{ter}} = E_{\mathrm{tot}}^{\mathrm{ter}} - \sum_i n_i \mu_i \quad (1)$$

Where $E_{\mathrm{f}}^{\mathrm{ter}}$ is the total energy of the supercell for each junction with each termination, n_i is the number of atoms of species *i* (Co, Fe, Ga, Ge, Mn, Si, or Ag), and μ_i are their chemical potentials. We assume that the chemical potential of the constituent atoms can be derived from bulk total energy of the single element per atom. エラー! 参照元が見つかりません。 illustrates the difference in formation energy between the two junctions for each interfacial termination. It is evident that the CMFS/Ag/CMFS(001) junction has lower formation energies across all interfacial terminations, indicating superior structural stability compared to the CFGG/Ag/CFGG(001) junction. Furthermore, Co terminations in both junctions show relatively higher formation energies than those of other junctions, suggesting that Co termination would be a metastable configuration. This introduces a potential uncertainty in experimental observations. However, theoretical predictions indicate that the FeGa and MnSi terminations are structurally more stable than the Co terminations at the CFGG/Ag and CMFS/Ag interfaces, respectively.

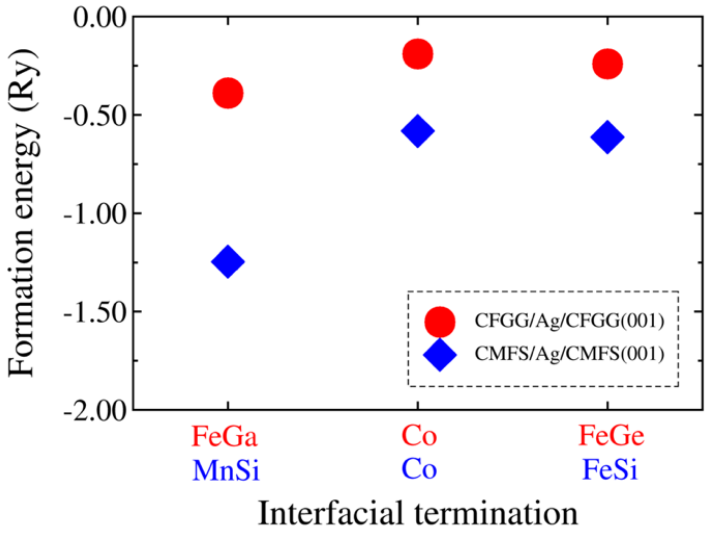

FIG. 2. Formation energies as a function of each interfacial termination comparing between $Co_2FeGa_{0.5}Ge_{0.5}$/Ag/$Co_2FeGa_{0.5}Ge_{0.5}$(001) and $Co_2Mn_{0.5}Fe_{0.5}Si$/Ag/$Co_2Mn_{0.5}Fe_{0.5}Si$(001) junctions.

B. Ballistic transport properties with the in-plane wave vector ($k_{||}$) dependence

To investigate the underlying physical factors contributing to the variation in transport properties between CFGG/Ag/CFGG(001) and CMFS/Ag/CMFS(001) junctions, we have performed calculations of the majority-spin conductance at the Fermi level in the parallel magnetization configuration. An average majority-spin conductance integrated over the two-dimensional Brillouin zone (2D BZ) of the in-plane wave vector $k_{||}$ of each interfacial termination for CFGG/Ag/CFGG(001) and CMFS/Ag/CMFS(001) junctions is depicted in エラー! 参照元が見つかりません。(a) and (b), respectively. Overall, the calculated majority-spin conductance using the CFGG electrode is larger than that using the CMFS electrode for all interfacial terminations, indicating a better Fermi surface matching of CFGG/Ag(001) than that of CMFS/Ag(001). Notably, the Co termination in both junctions exhibited the lowest conductance value among the terminations. The FeGe termination within the CFGG electrode presented the highest conductance value, while the Co termination within the CMFS electrode demonstrated the lowest conductance value.

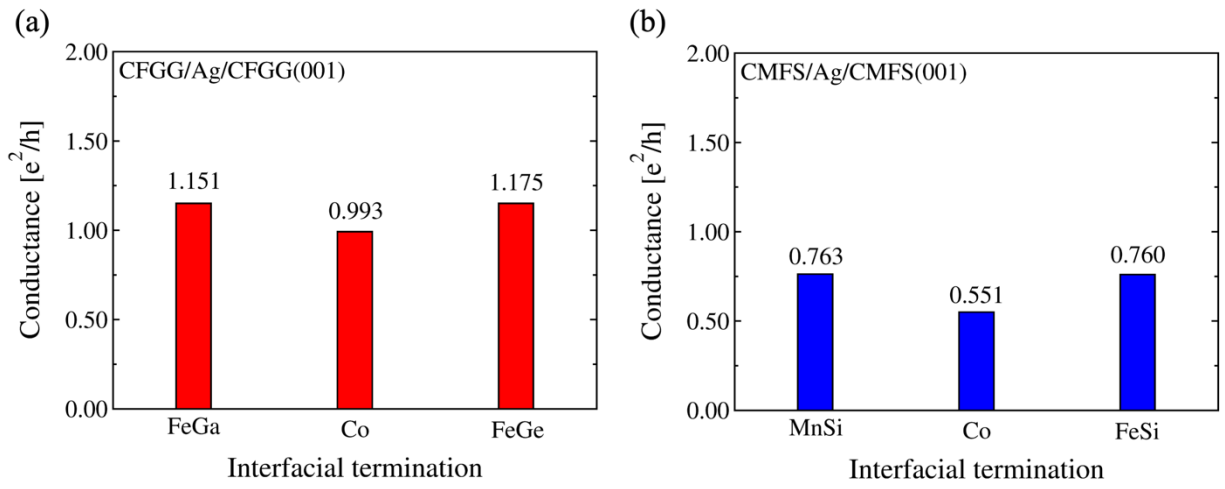

FIG. 3. A comparison of an average majority-spin conductance in the parallel magnetization of each interfacial termination for (a) $Co_2FeGa_{0.5}Ge_{0.5}$/Ag/$Co_2FeGa_{0.5}Ge_{0.5}$(001) and (b) $Co_2Mn_{0.5}Fe_{0.5}Si$/Ag/$Co_2Mn_{0.5}Fe_{0.5}Si$(001) junctions.

The $k_{\parallel}$ dependence of majority-spin conductance for each interfacial termination at the Fermi energy is shown within the 2D BZ for CFGG/Ag/CFGG(001) and CMFS/Ag/CMFS(001) junctions, in エラー! 参照元が見つかりません。(a-c) and エラー! 参照元が見つかりません。(d-f), respectively. Overall, the highly conductive regions (yellow-colored region) of ($k_{\parallel} = k_x, k_y$) strongly depend on the interfacial termination of the different electrodes at the two junctions. The CFGG/Ag/CFGG trilayers had a wider distribution of highly conductive regions compared to the CMFS/Ag/CMFS in the 2D $k_{\parallel}$ BZ. Around the Γ point ($k_{\parallel} = 0$), both CFGG and CMFS exhibited relatively very small conductance, with spreading occurring at $k_{\parallel}$ less than |0.25|. However, away from the Γ point ($k_{\parallel} \neq 0$), the highly conductive region of the CFGG electrode expanded significantly, while that of the CMFS electrode remained confined to a smaller region. These results indicate that the use of the CFGG electrode results in a lower majority-spin interface resistance area product ($R^{\uparrow}_{int.}A$) and a larger γ, leading to a higher magnetoresistance (MR) ratio compared to the use of the CMFS electrode.

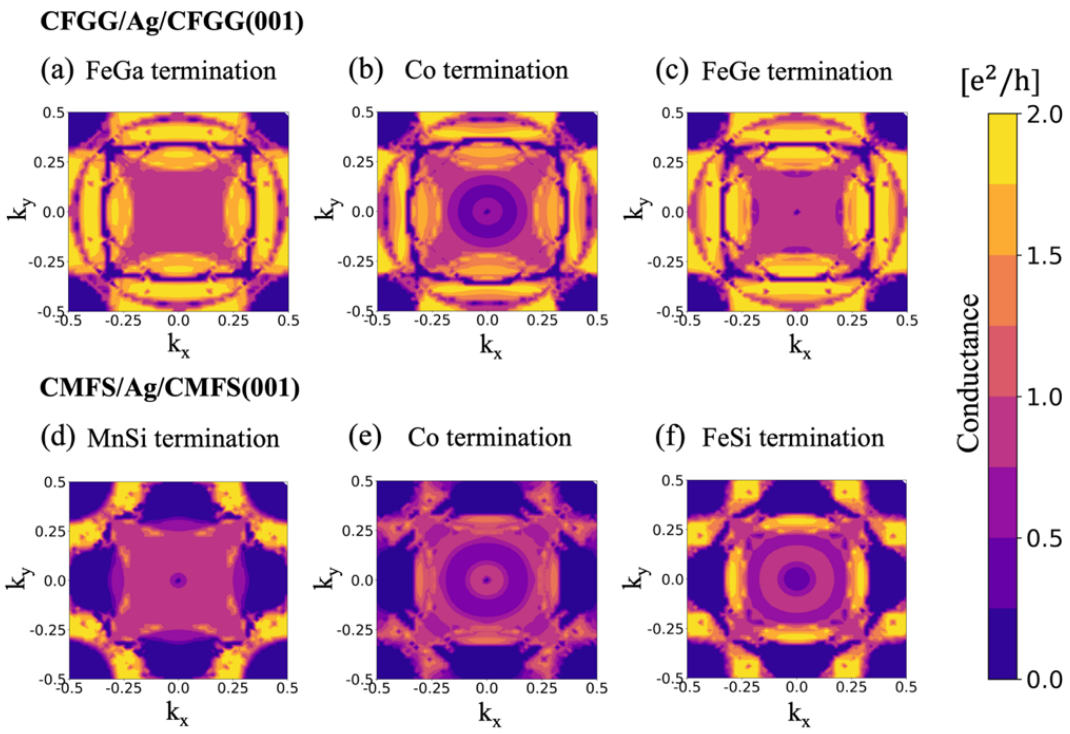

FIG. 4. In-plane wave vector $k_{\parallel} = (k_x, k_y)$ dependence of majority-spin conductance at the Fermi level in the parallel magnetization for $Co_2FeGa_{0.5}Ge_{0.5}$/Ag/$Co_2FeGa_{0.5}Ge_{0.5}$(001) junction with (a) FeGa termination, (b) Co termination, (c) FeGe termination and $Co_2Mn_{0.5}Fe_{0.5}Si$/Ag/ $Co_2Mn_{0.5}Fe_{0.5}Si$(001) junction with (d) MnSi termination, (e) Co termination, (f) FeSi termination.

In the ballistic regime, the conductance calculation is directly proportional to the number of conducting channels facilitating transport along to the current direction. To derive the intrinsic transport contributions, the normalization of the $R^{\uparrow}_{int.}A$ by the number of conducting channels [25] was considered by the following equation:

$$RA = \frac{Ah}{e^2}\left(\frac{1}{T} - \frac{1}{N}\right), \tag{2}$$

where A is the cross-sectional area, e is the elementary charge, h is the Planck's constant, T is the average of the transmission probability, and N is the average of the number of conducting channels.

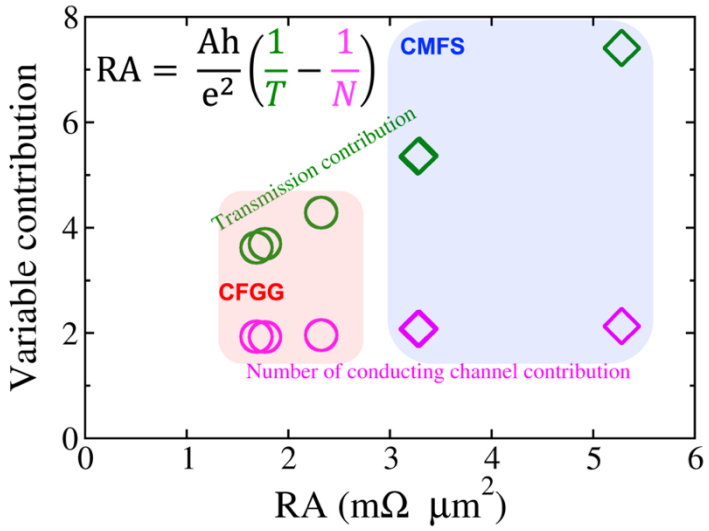

FIG. 5. Transmission and number of conducting channel contribution as a function of majority-spin resistance area product comparing between $Co_2FeGa_{0.5}Ge_{0.5}$/Ag/$Co_2FeGa_{0.5}Ge_{0.5}$(001) and $Co_2Mn_{0.5}Fe_{0.5}Si$/Ag/$Co_2Mn_{0.5}Fe_{0.5}Si$(001) junctions.

エラー! 参照元が見つかりません。 illustrates the plotted variable contributions, namely $\frac{1}{T}$ and $\frac{1}{N}$ as a function of the interface resistance area product normalization (*RA*). The primary contribution to both the CFGG and CMFS electrodes appears to come from the transmission probability of each channel. This suggests that the changing in the number of conducting channels between these two electrodes does not significantly affect their transport properties. As a result, the CFGG/Ag/CFGG(001) system consistently exhibits lower *RA* values across all terminations compared to the CMFS/Ag/CMFS(001) system, as shown in Table I. These theoretical *RA* values for the CFGG/Ag/CFGG(001) system agree well with previous research, confirming their lower values compared to the CMFS/Ag/CMFS(001) system, as reported in a previous study [22].

However, it should be noted that real materials may contain impurities, defects, or lattice imperfections that contribute to interface disorder. Consequently, interface disorder plays a critical role in determining the transport properties of materials. Nevertheless, in extremely pure and defect-free systems, where the mean free path of electrons is very long compared to the thickness of the NM spacer layer in CPP-GMR devices, the ballistic mode of transport can serve as a

reasonable approximation.

Interface disorder perturbs the electronic structure, often increasing the number of electronic bands crossing the Fermi level, which in turn creates additional scattering states and reduces the transmission of charge carriers compared to an ideal or pristine case. In our case study of ballistic electron transport, despite the presence of some disorder, the electron mean free path remains larger than the size of the structures, allowing conductance to remain ballistic and to arise from the change of the local potential and electronic structures at the interface. The exact values of conductance are material-dependent, highlighting the importance of understanding specific material characteristics when evaluating transport properties.

Table I Majority-spin resistance area product (RA) for $Co_2FeGa_{0.5}Ge_{0.5}$/Ag/$Co_2FeGa_{0.5}Ge_{0.5}$(001) and $Co_2Mn_{0.5}Fe_{0.5}Si$/Ag/$Co_2Mn_{0.5}Fe_{0.5}Si$(001) junctions of each interfacial termination.

Electrode	Interfacial termination	RA ($m\Omega\ \mu m^2$)
$Co_2FeGa_{0.5}Ge_{0.5}$	FeGa	1.77
	Co	2.32
	FeGe	1.69
$Co_2Mn_{0.5}Fe_{0.5}Si$	MnSi	3.27
	Co	5.28
	FeSi	3.29

C. Majority-spin conductance variation and Fermi surface matching

To gain deeper insight into the majority-spin conductance between CFGG/Ag/CFGG(001) and CMFS/Ag/CMFS(001), we examined the difference of the majority-spin conductance in the $k_{\parallel}$ space for identical interfacial terminations between the two electrodes, as shown in *エラー! 参照元が見つかりません。*(a-c). It was observed that there is a large difference in the highly conductive region around the BZ edge due to the CFGG electrode. These results indicate that the main causes of lower *RA* values are due to the higher conductive region around the BZ edge of CFGG/Ag/CFGG(001). In addition, Fermi surface analysis was performed for the tetragonal unit

cells of $L2_1$-$Co_2FeGa_{0.5}Ge_{0.5}$, fcc-Ag, and $L2_1$- $Co_2Mn_{0.5}Fe_{0.5}Si$, as visualized by XCRYDEN [29] in FIG. 6(d-f), respectively. Overall, the Fermi surface characteristics of CFGG and CMFS are comparable, but differences were found around the BZ edge. In this region, CMFS bulk electronic states lack energy levels for occupied or unoccupied electrons, indicating limited conductivity in CMFS materials. As a result, the CFGG electrode has the potential advantage of a larger conductive region around the BZ edge, leading to higher conductance compared to the CMFS electrode.

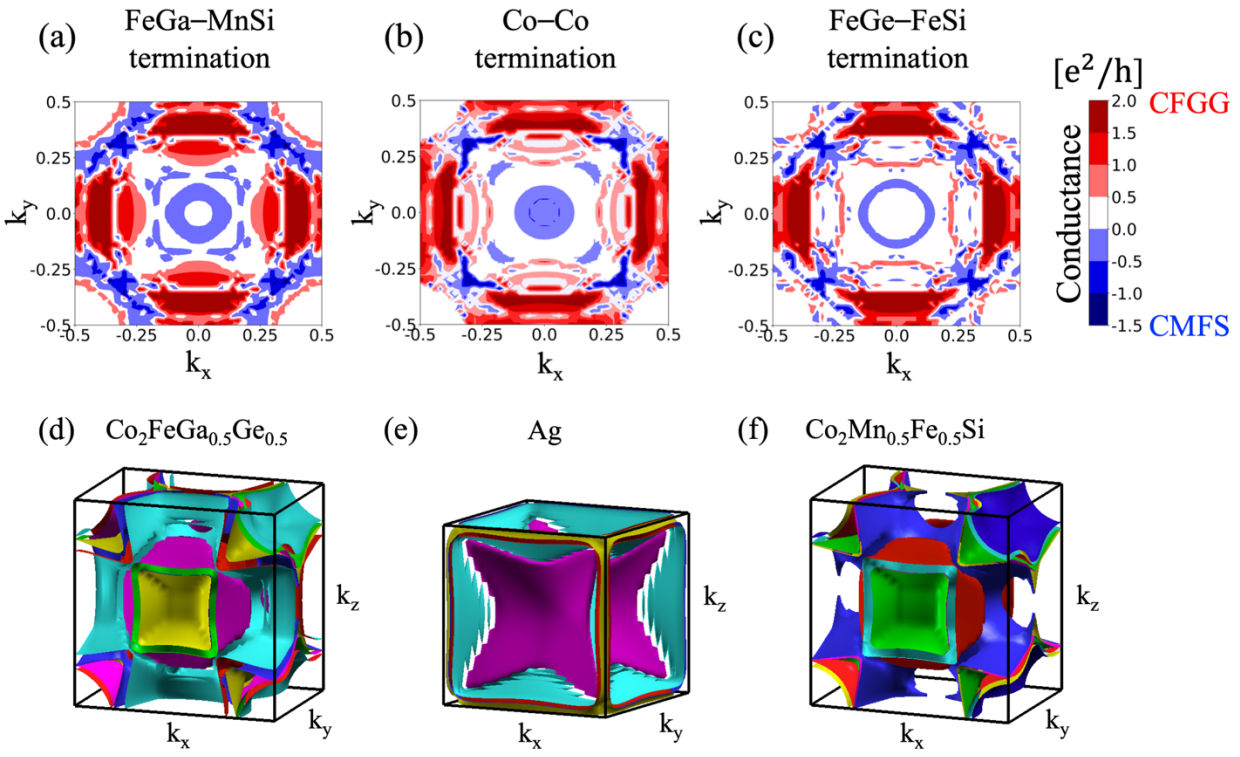

FIG. 6. Variation of majority-spin conductance in the parallel magnetization calculated between $Co_2FeGa_{0.5}Ge_{0.5}$/Ag/$Co_2FeGa_{0.5}Ge_{0.5}$(001) and $Co_2Mn_{0.5}Fe_{0.5}Si$/Ag/$Co_2Mn_{0.5}Fe_{0.5}Si$(001) for (a) FeGa-MnSi termination, (b) Co-Co termination, and (c) FeGe-FeSi termination. Fermi surface in the Brillouin zones corresponding to (d) the tetragonal unit cell of $L2_1$-$Co_2FeGa_{0.5}Ge_{0.5}$, (e) fcc-Ag, and (f) the tetragonal unit cell of $L2_1$-$Co_2Mn_{0.5}Fe_{0.5}Si$ visualized by XCRYDEN [29].

To gain a better understanding of the orbital contributions, the Fermi surfaces were separated into *s*, *p*, and *d* orbital compositions as visualized by FermiSurfer [36] in エラー! 参照

元が見つかりません。. The main contribution to the Fermi surface of the CFGG and CMFS bulk materials result from d orbital, followed by *p* and *s* orbitals. In contrast, the Ag bulk material shows a high contribution from the *p* orbital, followed by *d* and *s* orbitals, respectively. These results reveal a hybridization between the *d* states of the CFGG electrode and the *p* states of the Ag spacer around the BZ edge. This phenomenon is not observed for the CMFS electrode due to the lack of energy levels for occupied or unoccupied electrons, as previously mentioned. Consequently, the physical origin of the difference in their transport properties can be attributed to a strong distribution of highly conducting regions from the CFGG electrode around the BZ edge. This results from its superior Fermi surface matching at the BZ edge compared to the CMFS electrode, especially in terms of the *d* states of the CFGG electrode and the *p* states of the Ag spacer.

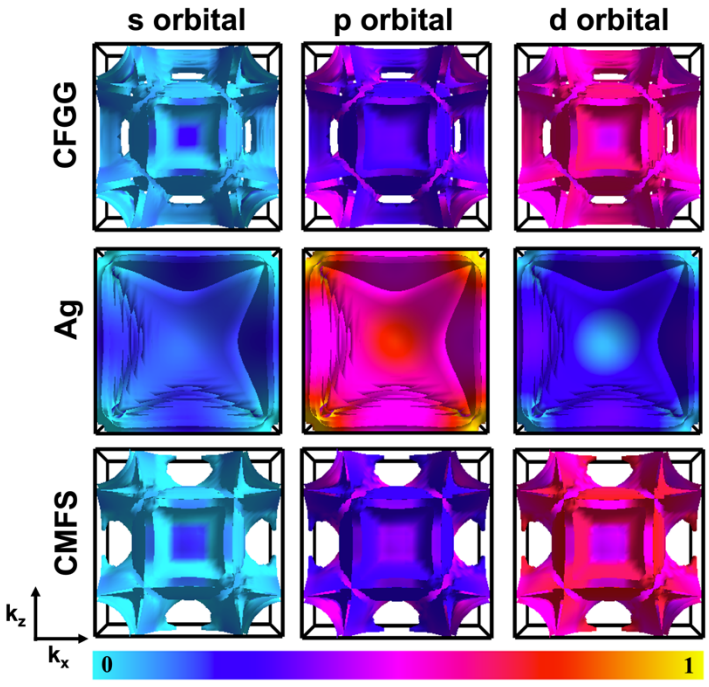

FIG. 7. Fermi surface separated into *s*, *p*, and *d* orbital compositions, where 0 and 1 values represent the ratio of each orbital contribution, for the tetragonal unit cell of $L2_1$-$Co_2FeGa_{0.5}Ge_{0.5}$, fcc-Ag, and the tetragonal unit cell of $L2_1$-$Co_2Mn_{0.5}Fe_{0.5}Si$ visualized by FermiSurfer [36].

D. Projected transmittance of a spacer and exchange stiffness at interface

To clarify the relevance of interfaces for the difference in the $k_{\parallel}$-dependence of the conductance, we have explicitly calculated the projection of the transmission coefficient ($|C_{\alpha lm}|$) on the local atomic orbital of the Ag spacer in the CFGG/Ag/CFGG(001) and CMFS/Ag/CFGG(001) trilayers at the Fermi level. Here, the α, l, and m are indices of atomic positions and local atomic orbitals, and the formulation of the $|C_{\alpha lm}|$ is given in Ref. [30]. This approach allows us to better understand the main contributions to the conducting behavior in these materials, as discussed in the previous section. As shown in Figs. 8(a) and (b), the main contribution to the transmittance over the $k_{\parallel}$ dependence comes from the Ag *d* orbitals, followed by the *p* and *s* orbitals, respectively, in both junctions. The presence of the *d* orbital feature at the interface is particularly interesting, indicating that the hybridization of the Co, Mn, and Fe *d* orbitals with Ag *d* orbital is a key factor in determining the $k_{\parallel}$-dependence of the transmittance. Furthermore, the transmittance feature over the $k_{\parallel}$ region at the interface is similar to the contribution of the highly conducting region in the overall systems (エラー! 参照元が見つかりません。). This also suggests that the majority-spin conductance of these junctions can be characterized by the *d* orbital of the Ag spacer at the interface. Furthermore, the main reason for the difference in conductance between the two junctions occurs around the Brillouin zone (BZ) edge, as evidenced by the *d* orbitals of the Ag spacer in both electrodes. Consequently, it should be noted that while the majority orbital contribution of the bulk Ag spacer comes from the *p* states, the *d* states play an important role in determining the $k_{\parallel}$-dependence of the transmittance at the interfaces.

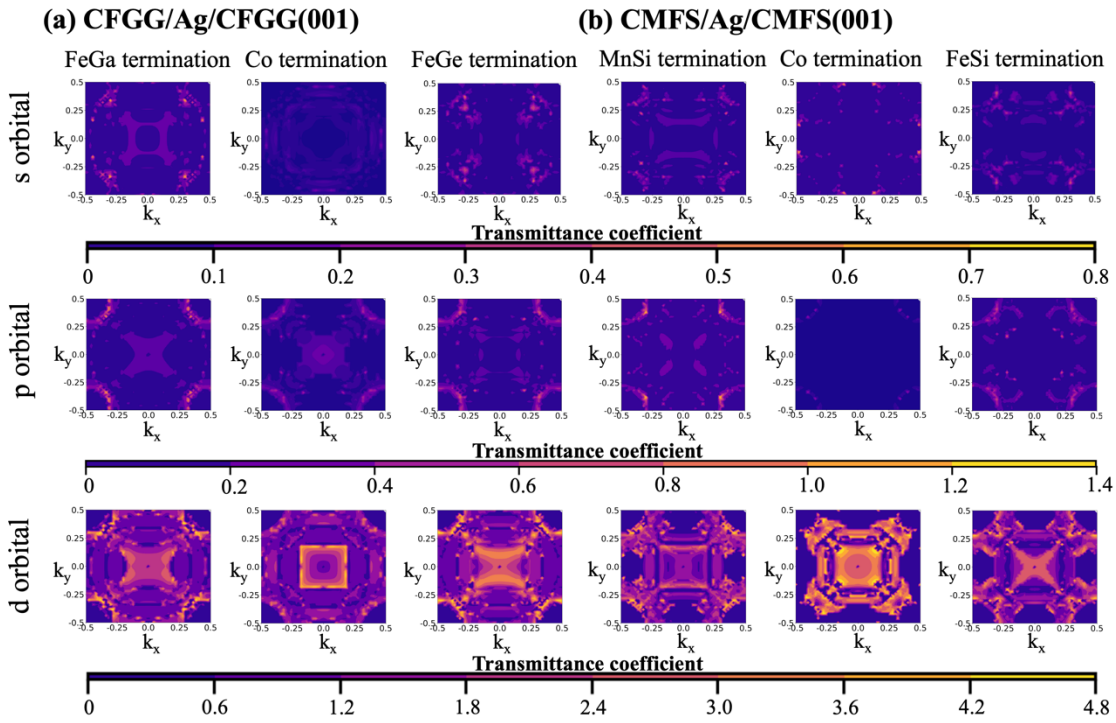

FIG. 8. Projected transmittance coefficient on the local atomic orbital of Ag spacer in the (a) $Co_2FeGa_{0.5}Ge_{0.5}$/Ag/$Co_2FeGa_{0.5}Ge_{0.5}$(001) and (b) $Co_2Mn_{0.5}Fe_{0.5}Si$/Ag/$Co_2Mn_{0.5}Fe_{0.5}Si$(001) trilayers at the Fermi level.

To further evaluate the efficiency of spin transport across the interface, we estimated the exchange stiffness constant at each interfacial termination of CFGG/Ag(001) and CMFS/Ag(001) junctions. This constant is a fundamental parameter characterizing the strength of the exchange interaction between neighboring magnetic moments in materials. The increase in the total energy of the system ($E(\theta)$) as a function of the angle of local spin moments (θ) was calculated. Subsequently, the function $E(\theta) = B(1 - \cos\theta)$ was employed to fit the obtained results using. Consequently, the inter-atomic layer exchange stiffness constant (B) was identified as illustrated in Table II. In addition, as shown in FIG. 9, the total energy increase as a function of tilting angle followed a quadratic trend ($\sim \theta^2$) up to $\theta = 15^{\circ}$. This implies that the error in estimating the exchange stiffness constant by the function $E(\theta) = B(1 - \cos\theta)$ is negligible in the present system [37].

Table II Exchange stiffness constant B [meV/*uca*] fitted to the increase in energies, $E(\theta) = B(1 - \cos\theta)$, due to the noncollinearity of local spin moments for CFGG/Ag(001) and CMFS/Ag(001) junctions. The unit-cell area (*uca*) is approximately 33 $Å^2$ for CFGG and 32 $Å^2$ for CMFS.

B (meV/*uca*)	Interfacial termination of CFGG/CMFS electrodes		
	FeGe/FeSi	Co/Co	FeGa/MnSi
CFGG/Ag(001)	134	115	129
CMFS/Ag(001)	113	134	105

Overall, the exchange stiffness constant of the CFGG/Ag(001) interface was significantly larger than that of the CMFS/Ag(001) interface (Table II), except that the Co termination has a lower exchange stiffness constant compared to that in CMFS/Ag(001) interface. With the stronger exchange interaction at the CFGG/Ag(001) interface, the interfacial magnetic moments are more constrained and less likely to fluctuate at finite temperatures. Conversely, the weaker interaction at the CMFS/Ag(001) allows for easier fluctuations of the interfacial magnetic moments. Among various terminations of the CFGG/Ag(001) and the CFMS/Ag(001) interfaces, the FeGe and Co termination, respectively, exhibit the largest and comparable exchange stiffness constant of 134 meV/uca (FIG. 9). In contrast, the instability of spin moments against thermal agitation was found at the MnSi interfacial termination in the CMFS/Ag(001) interface, with the lowest exchange stiffness constant of 105 meV/uca (FIG. 9). Considering the highest structural stability of each electrode, indicated by the formation energy as discussed in section A, the FeGa termination in CFGG/Ag(001) interface provides a higher exchange stiffness constant compared to the MnSi termination in CMFS/Ag(001) interface. This suggests a higher stability of the spin moment against thermal agitation. Consequently, the CFGG electrode exhibited not only a higher majority-spin conductance leading to a higher MR ratio but also a higher stability of spin moment against thermal fluctuations, thereby suppressing the reduction of the MR ratio at finite temperatures compared to the CMFS electrode.

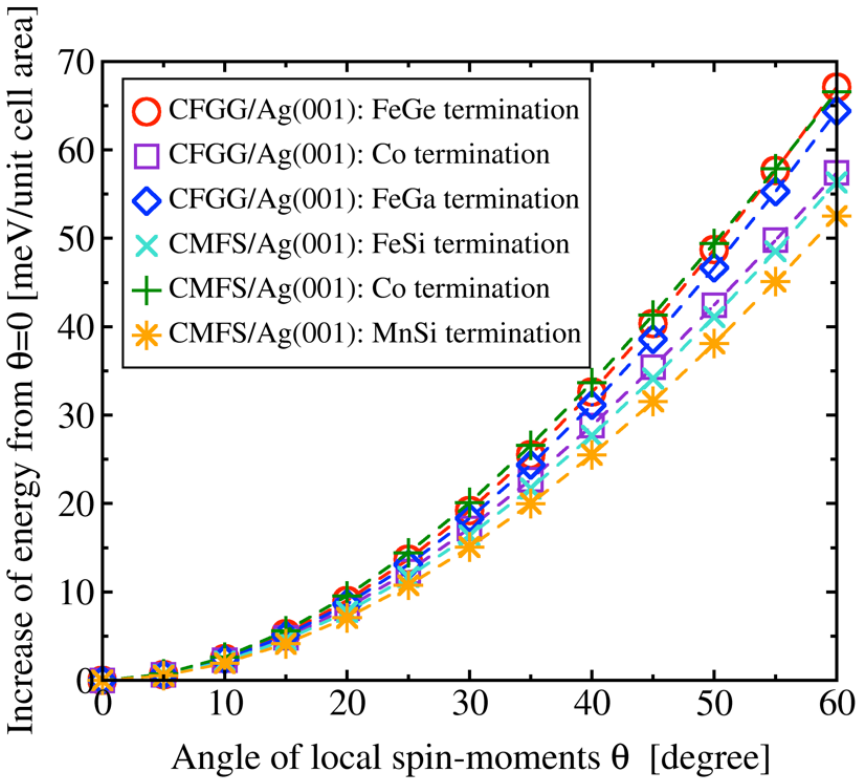

FIG. 9. Increase in the total energy relative to the collinear-spin system, $E(\theta)$, as a function of the angle of local spin moments, θ, for various interfacial terminations of CFGG/Ag(001) and CMFS/Ag(001) junctions.

IV. SUMMARY

In this paper, we perform first-principles ballistic transport calculations based on the Landauer formula to clarify the physical origins of the spin-dependent transport properties between CFGG/Ag/CFGG(001) and CMFS/Ag/CMFS(001) junctions. First, we determined the structural stability of interfaces for the two different electrodes by comparing their formation energies. The results showed that the CMFS/Ag/CMFS(001) junctions exhibited lower formation energies among all interfacial terminations, suggesting superior structural stability compared to the CFGG/Ag/CFGG(001) junctions. Secondly, the difference in transport properties was investigated. The CFGG/Ag/CFGG trilayers showed a more widespread distribution in the majority-spin conductance in the 2D $k_{\parallel}$ Brillouin zone compared to CMFS/Ag/CMFS. In particular, the highly conductive distribution for the CFGG electrode expanded significantly around the BZ edge, which

was not observed in the CMFS electrode. This indicated a lower majority-spin interface resistance area product ($R_{\mathrm{int.}}^{\uparrow}\mathrm{A}$) and implied a higher Magnetoresistance (MR) output for the CFGG/Ag/CFGG(001) system compared to the CMFS/Ag/CMFS(001) system. We then elucidated the difference in the $k_{\parallel}$ dependence of the majority-spin conductance by investigating the projected transmittance on the local atomic orbital of the Ag spacer at the interface of the magnetic junctions. We found that the *d* orbital feature at the interface in the $k_{\parallel}$ dependence is similar to the conducting contribution in the whole systems, indicating that the majority of conducting channels originate from the *d* orbital of the Ag spacer at the interface. This presence of the *d* orbital feature at the interface is particularly interesting. This implies that the hybridization of Co, Mn, and Fe *d* orbitals with Ag *d* orbital plays a crucial role in determining the $k_{\parallel}$-dependence of the transmittance. Furthermore, a high transmittance was found around the BZ edge, which contributed significantly to the different conducting regions in the $k_{\parallel}$ BZ between the two electrode configurations. Finally, the exchange stiffness constant was estimated and showed that most interfacial terminations in the CFGG/Ag(001) interfaces have higher stability of local spin moments for thermal fluctuations than that in the CMFS/Ag(001) interfaces. This stability is essential for suppressing the spin-flip scattering and for maintaining the MR ratio despite thermal fluctuations of magnetization at finite temperatures. The present findings suggest that the CFGG electrode will be suitable for larger CPP-GMR at room temperature which is worthy of further investigation.

ACKNOWLEDGMENTS

This work was supported by JSPS KAKENHI Grant No. 21H01608, MEXT Initiative to Establish Next-generation Novel Integrated Circuits Centers (X-NICS) Grant No. JPJ011438, MEXT Program: Data Creation and Utilization-Type Material Research and Development Project (Digital Transformation Initiative Center for Magnetic Materials; Grant No. JPMXP1122715503), and JST CREST (Grant No. JPMJCR21O1). The high-performance computing resources provided by the National Institute for Materials Science (NIMS) Numerical Materials Simulator are gratefully acknowledged. We thank all members of the Spin Theory Group and Magnetic Functional Device Group at NIMS, particularly Dr. Ivan Kurniawan and Dr. Hirofumi Suto, for the fruitful discussion.

REFERENCES

[1] V. K. N. V. A. Jogo, V. T. Ibusuki, V. H. O. V. Y. Shimizu, and V. T. Uzumaki, *CPP-GMR Technology for Future High-Density Magnetic Recording*, Fujitsu Sci Tech J **42**, 149 (2006).

[2] M. Takagishi, K. Yamada, H. Iwasaki, H. N. Fuke, and S. Hashimoto, *Magnetoresistance Ratio and Resistance Area Design of CPP-MR Film for 2–5 $\hbox{Tb/In}^{2}$ Read Sensors*, IEEE Trans. Magn. **46**, 2086 (2010).

[3] S.-F. Lee, W. P. Pratt, Q. Yang, P. Holody, R. Loloee, P. A. Schroeder, and J. Bass, *Two-Channel Analysis of CPP-MR Data for Ag/Co and AgSn/Co Multilayers*, J. Magn. Magn. Mater. **118**, L1 (1993).

[4] T. Valet and A. Fert, *Theory of the Perpendicular Magnetoresistance in Magnetic Multilayers*, Phys. Rev. B **48**, 7099 (1993).

[5] Y. K. Takahashi, A. Srinivasan, B. Varaprasad, A. Rajanikanth, N. Hase, T. M. Nakatani, S. Kasai, T. Furubayashi, and K. Hono, *Large Magnetoresistance in Current-Perpendicular-to-Plane Pseudospin Valve Using a Co2Fe(Ge0.5Ga0.5) Heusler Alloy*, Appl. Phys. Lett. **98**, 152501 (2011).

[6] O. M. Chumak, A. Nabiałek, R. Zuberek, I. Radelytskyi, T. Yamamoto, T. Seki, K. Takanashi, L. T. Baczewski, and H. Szymczak, *Magnetoelastic Properties of Epitaxially Grown Co2Fe0.4Mn0.6Si and Co2FeGa0.5Ge0.5 Heusler Alloys Thin Films*, IEEE Trans. Magn. **53**, 1 (2017).

[7] L. Bainsla, K. Z. Suzuki, M. Tsujikawa, H. Tsuchiura, M. Shirai, and S. Mizukami, *Magnetic Tunnel Junctions with an Equiatomic Quaternary CoFeMnSi Heusler Alloy Electrode*, Appl. Phys. Lett. **112**, 052403 (2018).

[8] O. M. Chumak et al., *Magnetoelastic Interactions and Magnetic Damping in Co2Fe0.4Mn0.6Si and Co2FeGa0.5Ge0.5 Heusler Alloys Thin Films for Spintronic Applications*, Sci. Rep. **11**, 7608 (2021).

[9] K. B. Fathoni, Y. Sakuraba, Y. Miura, T. Sasaki, T. Nakatani, and K. Hono, *Analysis of Current-in-Plane Giant Magnetoresistance Using Co2FeAl0.5Si0.5 Half-Metallic Heusler Alloy*, J. Phys. Appl. Phys. **55**, 125001 (2021).

[10] Z. Chen, Y. Sakuraba, Y. Miura, Z. Li, T. Sasaki, H. Suto, V. K. Kushwaha, T. Nakatani, S. Mitani, and K. Hono, *Phase Stability and Half-Metallic Character of off-Stoichiometric Co2FeGa0.5Ge0.5 Heusler Alloys*, J. Appl. Phys. **132**, 183902 (2022).

[11] Y. Sakuraba, K. Izumi, T. Iwase, S. Bosu, K. Saito, K. Takanashi, Y. Miura, K. Futatsukawa, K. Abe, and M. Shirai, *Mechanism of Large Magnetoresistance in \textCo_2\textMnSi/\textAg/\textCo_2\textMnSi Devices with Current Perpendicular to the Plane*, Phys Rev B **82**, 094444 (2010).

[12] T. Iwase, Y. Sakuraba, S. Bosu, K. Saito, S. Mitani, and K. Takanashi, *Large Interface Spin-Asymmetry and Magnetoresistance in Fully Epitaxial Co2MnSi/Ag/Co2MnSi Current-Perpendicular-to-Plane Magnetoresistive Devices*, Appl. Phys. Express **2**, 063003 (2009).

[13] Y. Sakuraba, M. Ueda, Y. Miura, K. Sato, S. Bosu, K. Saito, M. Shirai, T. J. Konno, and K. Takanashi, *Extensive Study of Giant Magnetoresistance Properties in Half-Metallic Co2(Fe,Mn)Si-Based Devices*, Appl. Phys. Lett. **101**, 252408 (2012).

[14] T. Kubota, Y. Ina, Z. Wen, and K. Takanashi, *Temperature Dependence of Current-Perpendicular-to-Plane Giant Magnetoresistance in the Junctions with Interface Tailored Heusler Alloy Electrodes*, J. Magn. Magn. Mater. **474**, 365 (2019).

[15] Y. Fujita, Y. Miura, T. Sasaki, T. Nakatani, K. Hono, and Y. Sakuraba, *Spin-Scattering Asymmetry at Half-Metallic-Ferromagnet|ferromagnet Interface*, Phys. Rev. B **104**, L140403 (2021).
[16] S. Li, Y. K. Takahashi, T. Furubayashi, and K. Hono, *Enhancement of Giant Magnetoresistance by L21 Ordering in Co2Fe(Ge0.5Ga0.5) Heusler Alloy Current-Perpendicular-to-Plane Pseudo Spin Valves*, Appl. Phys. Lett. **103**, 042405 (2013).
[17] J. W. Jung, Y. Sakuraba, T. T. Sasaki, Y. Miura, and K. Hono, *Enhancement of Magnetoresistance by Inserting Thin NiAl Layers at the Interfaces in Co2FeGa0.5Ge0.5/Ag/Co2FeGa0.5Ge0.5 Current-Perpendicular-to-Plane Pseudo Spin Valves*, Appl. Phys. Lett. **108**, 102408 (2016).
[18] B. Büker, J. Jung, T. Sasaki, Y. Sakuraba, Y. Miura, T. Nakatani, A. Hütten, and K. Hono, *Elucidation of the Strong Effect of an Interfacial Monolayer on Magnetoresistance in Giant Magnetoresistive Devices with Current Perpendicular to the Plane*, Phys. Rev. B **103**, L140405 (2021).
[19] A. Fert, T. Valet, and J. Barnas, *Perpendicular Magnetoresistance in Magnetic Multilayers: Theoretical Model and Discussion (Invited)*, J. Appl. Phys. **75**, 6693 (1994).
[20] J. Barnas, and A. Fert, *Interface Resistance for Perpendicular Transport in Layered Magnetic Structures*, Phys Rev B **49**, 12835 (1994).
[21] K. Yakushiji, K. Saito, S. Mitani, K. Takanashi, Y. K. Takahashi, and K. Hono, *Current-Perpendicular-to-Plane Magnetoresistance in Epitaxial Co2MnSi/Cr/Co2MnSi Trilayers*, Appl. Phys. Lett. **88**, 222504 (2006).
[22] Y. Miura, *First-Principles Studies on Spin-Dependent Transport of Magnetic Junctions with Half-Metallic Heusler Compounds*, J. Magn. Soc. Jpn. **47**, 90 (2023).
[23] Q. Yang, P. Holody, R. Loloee, L. L. Henry, W. P. Pratt, P. A. Schroeder, and J. Bass, *Prediction and Measurement of Perpendicular Giant Magnetoresistances of Co/Cu/${\mathrm{Ni}}_{84}${\mathrm{Fe}}_{16}$/Cu Multilayers*, Phys. Rev. B **51**, 3226 (1995).
[24] S.-F. Lee et al., *Current-Perpendicular and Current-Parallel Giant Magnetoresistances in Co/Ag Multilayers*, Phys. Rev. B **52**, 15426 (1995).
[25] K. M. Schep, J. B. A. N. van Hoof, P. J. Kelly, G. E. W. Bauer, and J. E. Inglesfield, *Interface Resistances of Magnetic Multilayers*, Phys. Rev. B **56**, 10805 (1997).
[26] R. Landauer, *Electrical Resistance of Disordered One-Dimensional Lattices*, Philos. Mag. J. Theor. Exp. Appl. Phys. **21**, 863 (1970).
[27] J. P. Perdew, K. Burke, and M. Ernzerhof, *Generalized Gradient Approximation Made Simple*, Phys. Rev. Lett. **77**, 3865 (1996).
[28] S. Baroni, A. dal Corso, S. de Gironcoli, and P. Giannozzi, *URL Http://Www. Pwscf. Org/.*, Google Sch. There No Corresp. Rec. This Ref. (2008).
[29] A. Kokalj, *Computer Graphics and Graphical User Interfaces as Tools in Simulations of Matter at the Atomic Scale*, Proc. Symp. Softw. Dev. Process Mater. Des. **28**, 155 (2003).
[30] H. Joon Choi and J. Ihm, *Ab Initio Pseudopotential Method for the Calculation of Conductance in Quantum Wires*, Phys. Rev. B **59**, 2267 (1999).
[31] A. Smogunov, A. Dal Corso, and E. Tosatti, *Ballistic Conductance of Magnetic Co and Ni Nanowires with Ultrasoft Pseudopotentials*, Phys. Rev. B **70**, 045417 (2004).
[32] G. Kresse and J. Furthmüller, *Efficiency of Ab-Initio Total Energy Calculations for Metals and Semiconductors Using a Plane-Wave Basis Set*, Comput. Mater. Sci. **6**, 15 (1996).

[33] G. Kresse and J. Furthmüller, *Efficient Iterative Schemes for Ab Initio Total-Energy Calculations Using a Plane-Wave Basis Set*, Phys. Rev. B **54**, 11169 (1996).
[34] M. Weinert, R. E. Watson, and J. W. Davenport, *Total-Energy Differences and Eigenvalue Sums*, Phys. Rev. B **32**, 2115 (1985).
[35] G. H. O. Daalderop, P. J. Kelly, and M. F. H. Schuurmans, *First-Principles Calculation of the Magnetocrystalline Anisotropy Energy of Iron, Cobalt, and Nickel*, Phys. Rev. B **41**, 11919 (1990).
[36] M. Kawamura, *FermiSurfer: Fermi-Surface Viewer Providing Multiple Representation Schemes*, Comput. Phys. Commun. **239**, 197 (2019).
[37] S. Lounis and P. H. Dederichs, *Mapping the Magnetic Exchange Interactions from First Principles: Anisotropy Anomaly and Application to Fe, Ni, and Co*, Phys. Rev. B **82**, 180404 (2010).